Applied Physics A (2022) 128:523
https://doi.org/10.1007/s00339-022-05605-x

Applied Physics A
Materials Science & Processing

Room-temperature nitrogen dioxide gas sensor based on graphene oxide nanoribbons decorated with MoS_2 nanospheres

Mehrafagh Rigi Jangjoo[1] · **M. Berahman**[1]

Received: 24 November 2021 / Accepted: 15 April 2022 / Published online: 24 May 2022

Abstract

Nitrogen dioxide (NO_2) has harmful effects on human health as well as the environment, and hence, developing low cost and power consumption of NO_2 sensors is of great importance. Combed shape gold electrodes sputtered on the surface of silicon substrate were modified with narrow graphene oxide nanoribbons and MoS_2 nanospheres to fabricate the gas sensor; synthesized by longitudinal unzipping of carbon nanotubes. Under static conditions and room temperature, we could detect NO_2 with concentrations as low as ten ppm with 33% and 250% sensitivity for pristine and MoS_2-decorated graphene oxide nanoribbon thin film, respectively. The gas-sensing mechanism has been studied using density functional theory in combination with XRD, TEM, SEM, FTIR, and Raman results. In the case of pristine graphene oxide nanoribbons, detection is based on the adsorption of gas molecules at the defect sites and charge transfer of the molecules. In contrast, the charge transfer and change in the Schottky barrier are dominant in the decorated sensor. These results are expected to provide new perspectives toward detecting of nitrogen dioxide on the surface of MoS_2 nanospheres@graphene oxide nanoribbon-modified electrodes with a low detection limit.

✉ M. Berahman
m.berahman@kgut.ac.ir

[1] Department of Electrical and Computer Engineering, Graduate University of Advanced Technology, Kerman, Iran

Graphical abstract

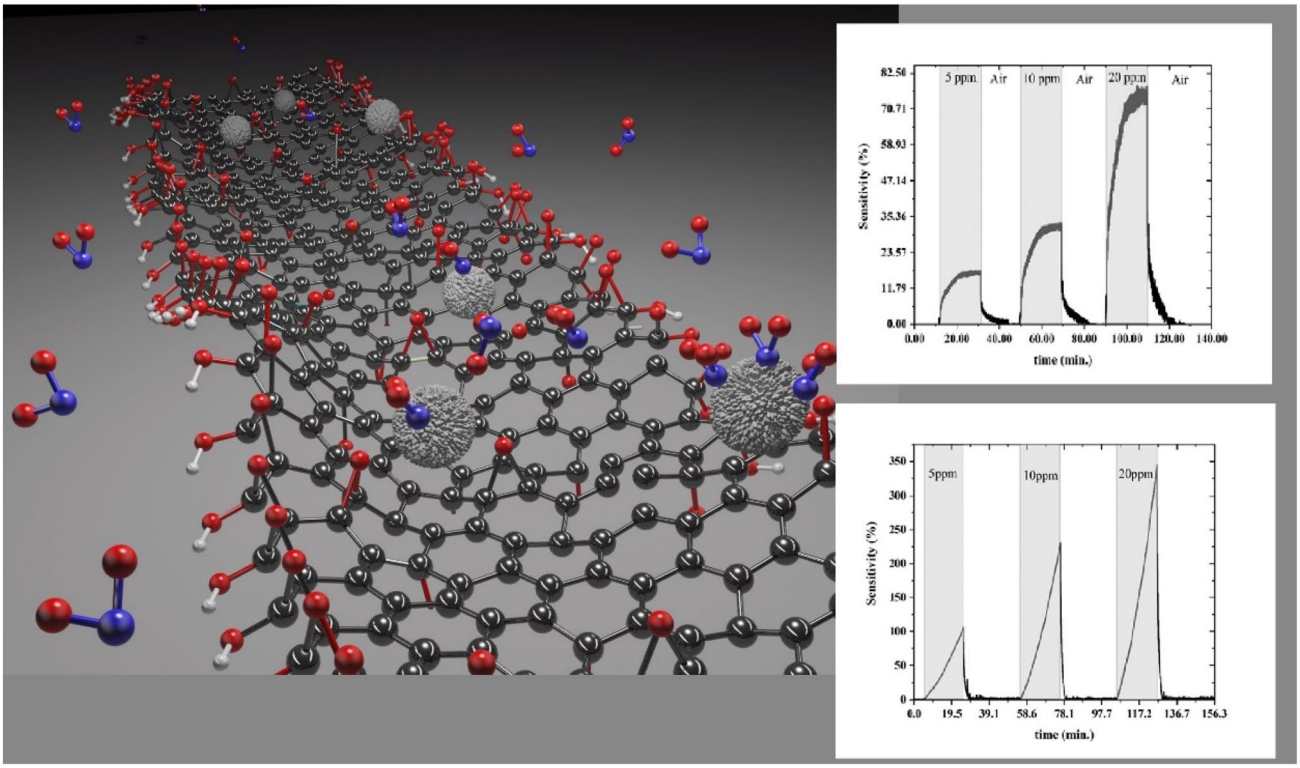

Keywords Nitrogen dioxide · Gas sensor · Graphene oxide nanoribbon · MoS_2 nanospheres

1 Introduction

Nitrogen dioxide (NO_2) gas has significant harmful effects on human health and the environment. Prolong exposure to even a small concentration (on the order of 10 ppm) of this gas can cause severe asthma symptoms, lung infections, and throat irritation [1]. In contrast, its high-level concentration can harm vegetables and decrease their growth and yields. Hence, monitoring the level of NO_2 concentration in the environment, and developing a gas sensor with low power consumption and cost along with high compatibility with current electronic technology is highly required [2]. Numerous reports developed smart gas sensors to detect air quality on the Internet of Thing (IoT) technology, and one of the main concerns is detecting the level of NO_2 concentration. In this regard, several techniques have been proposed to achieve such demand. One of the promising ones is to utilize low-dimensional materials capable of gas sensing at room temperature.

Graphene nanoribbon (GNR), a nano-strip of graphene, has recently been used for different applications, including but not limited to energy storage [3], nanocoating [4], membrane separation [5], transistor [6, 7], and even solar cells [8–10]. Excellent chemical and physical properties of GNRs such as controllable bandgap, large surface-to-volume ratio, tunable electrical properties, dopant control, and edge functionalization turn GNRs into a remarkable candidate for single gas molecule detection applications [11–15]. Controlling these properties needs a proper technique to synthesize GNRs, and there are numerous reports on such goals [13–18]. Longitudinal unzipping of carbon nanotubes in an oxidative medium is considered as one of the main techniques leading to narrow graphene oxide nanoribbons (GONRs) [17, 18].

GONRs possess oxygen functional groups such as hydroxyl and carboxyl on their surface, in addition to defects produced during the process of fabrication [17, 18]. These defects and dangling bonds have sp^2 hybridization. They are considered as active sites of electron transfer for detecting gas molecules besides other capabilities which improve the sensing behavior of pristine GNR [19–26]. Numerous reports can be found using GONRs for electrochemical detection of various electroactive substances and biomarkers, including ascorbic acid, dopamine, and uric acid [19, 20], glucose [21], cholesterol [22], amino acid biomarker [23], and Parkinson [24]. Also, detecting an acceptable

amount of hydrogen peroxide [25] and ethanol [26] has been reported.

Previous studies have revealed that composites of GNR with other functional nanomaterials can improve its characteristic to detect a low concentration of gases to a great extent. For instance, Wang et al. reported on ZnO nanoparticle-decorated GONRs for the detection of nitrogen dioxide with a detection limit of 50 ppm with 18% sensitivity [27]. In another study, adding WS_2 nanoflakes to GONRs is investigated to detect ethanol [28]. Recently, fire detection is also reported using GONRs [29]. Hence, combining GONRs with other nanoparticles can enhance detecting NO_2, and one of the promising nanoparticles for such demand is MoS_2.

MoS_2 nanoparticle has been reported as an attractive substrate for detecting gas molecules such as NO_2 and NH_3 [30]. Our previous work demonstrates the potential of flower-shaped MoS_2 nanoflakes in detecting methanol and xylene [31]. Hydrothermal has been used to grow flower-shaped MoS_2 for detecting the NO_2 at 100 °C with 10% sensitivity [32]. For 10 ppm at room temperature, using In_2O_3 [33] or MoO_3 [34] with these flower-shaped MoS_2 improves the sensitivity of detecting the NO_2 to 20% and 33.6%, respectively. These reports demonstrate the potential of flower-shaped MoS_2 nanoparticles while representing the importance of combining them with the other materials. These reports also revealed that transfer of charge from gas to MoS_2 is large, but the transfer of electric charge to the electrodes is not proper. While the detection is good in MoS_2 theoretically, the experiments do not show such a thing, which relate to lack of proper transferring electric charges to the electrodes. Adding a material that both detect NO_2 and also can transmit charge to the electrodes properly may improve the sensitivity and gas detection of the flower-shaped MoS_2. Using GONRs with MoS_2 may act adequately as a solution for such a problem.

First, we consider the GONR thin film to detect the low-level NO_2 gas molecules in the static environment at room temperature. Then, by combining theoretical and experimental investigations, the adsorption mechanism was studied. To assess the effect of MoS_2–GONR heterojunction in constructing gas sensors, decorated GONRs with flower-shape MoS_2 nanospheres have been used to detect NO_2 gas molecules. Using a Density Functional Theory (DFT) simulation model, the mechanism of such detection is investigated.

2 Materials and methods

2.1 Graphene oxide nanoribbon preparation

GONRs were synthesized via longitudinal unzipping of MWCNTs, as previously reported [18]. In short, a 300 mg portion of MWCNTs (Neutrino Co.) was dispersed in H_2SO_4 (72 mL) and stirred for an hour. Then, 8 mL of phosphoric acid (H_3PO_4 85%) with $KMnO_4$ (8 wt%, 2.4 g) was added to the solution while stirring continued for 15 min. Next, the solution was kept at 65 °C for 2 h. At this point, the black solutions turn into dark brown. Finally, the solutions were centrifuged, washed, and dried.

2.2 Synthesis of MoS_2 nanosphere

The detail of synthesizing MoS_2 nanospheres composed of few-layer sheets was reported before [35]. First, a mix of 0.15 g MoO_3 powder and 0.13 g thiourea with 40 mL deionized water is stirred for half an hour. Then, the result solution was kept at 200 °C for 32 h in an autoclave. Finally, the black product is filtered and washed several times to reach proper MoS_2 nanospheres.

2.3 Characterization

The Bruker D8 Advance X-Ray with a CuK_α source (wavelength $\lambda = 0.154185$ nm) was used to obtain X-ray diffraction (XRD). Sample morphology was characterized by transmission electron microscopy (MIRA3). The Fast Fourier IR spectrum is obtained using TENSOR II–Bruker FITR. Field-emission scanning electron microscopy (FE-SEM, TESCAN, MIRA3) was used to characterize sample morphology. The Raman characterization of thin-film layers is done using TEKSAN FirstGuard Raman Analyzer with 532 nm laser beam wavelength.

2.4 Device fabrication

For the sensor fabrication, a <100> p-type silicon has been used with a 200 nm silicon oxide layer as substrate. First, the substrate was clean from undesirable surface contaminants using isopropyl alcohol. Then, the combed shape electrodes were fabricated using a 150 nm gold layer with 2 nm Ti sputtered using a shadow mask on the surface of the substrate. Finally, the dispersed solution of GONR (0.1 mg/mL) was drop cast on the comb shape electrodes and heated till dry. For the construction of MoS_2 nanospheres@graphene oxide nanoribbons thin film, MoS_2 suspension with a concentration of 1 mg/mL was cast on the dried layer of GONR thin film. The inset of Fig. 1 shows the schematic and the actual sensor before and after the final drop cast.

2.5 Gas sensing

The gas-sensing characteristics of the samples perform using a homemade setup, as shown in Fig. 1. The gas concentrations were controlled by changing the mixing ratio of examined gas and N_2 regulated by two Alicat Scientific mass flow controllers. Both gases were mixed in the gas mixer

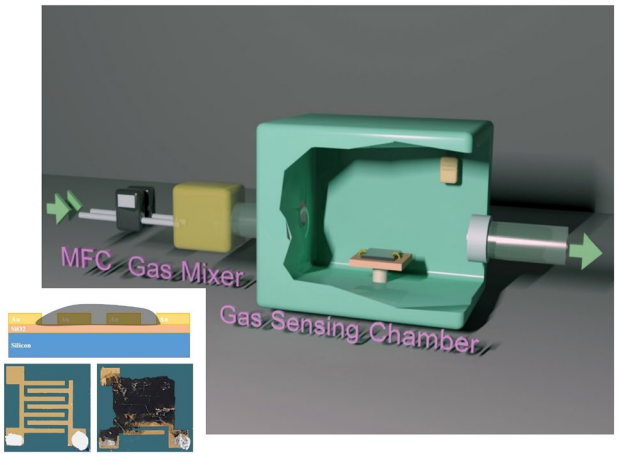

Fig. 1 The schematic diagram of the gas sensing setup. The inset shows the schematic of the fabricated gas sensor and the final sensor

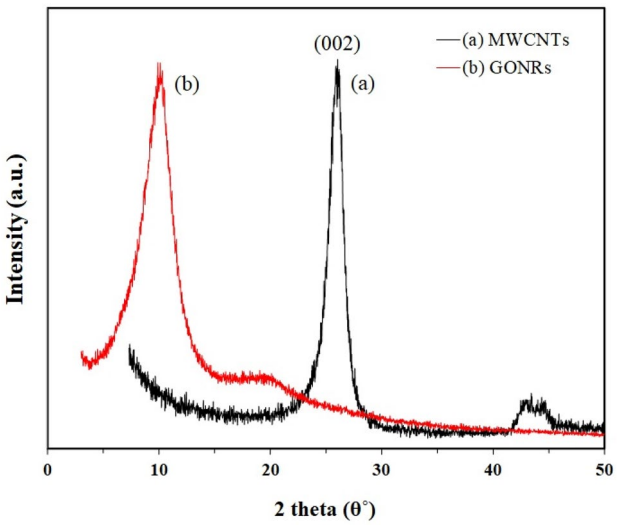

Fig. 2 The XRD of MWXCNT and GONRs in black and red curves, respectively

and entered the sensing chamber. A constant bias voltage of 0.5 V is applied to the designed sensor, and electrical resistance is measured by a proper multimeter. The chamber is designed, so the tested sensor is in the temperature range of 23–25 °C with humidity in a 5–7% environment. To test the sample toward different gas molecules, first, the chamber is flushed with dry-N_2 gas to clean it. Then, the sensing chamber is filled with dry-N2, and the sensor is rested for 10 min. in it. Next, the tested concentration of examined gas enters the chamber for the requested time as described. Finally, dry-N_2 is used for the recovery of the sensor. A simple circuit using proper series resistance is used to detect the sensor's resistance. Special care must be done on the electric current through the sensor, since an increase in the electric current may increase the temperature of the GONR thin film and affect the results. The chemoresistance response is defined as follows:

$$\text{Sensor Response} = \frac{R_{\text{gas}} - R_{\text{air}}}{R_{\text{air}}} \times 100. \quad (1)$$

In Eq. 1, R_{air} and R_{gas} are the resistance of the designed sensor before and after exposure to the target gas molecules, respectively.

3 Simulation

Density functional theory was used to simulate the electrical characteristic in this study as implemented in the well-known Siesta package [36, 37]. The Generalized Gradient Approximation with a Perdew–Burke–Ernzerhof correlation function was considered as exchange correlation. In addition, double-ζ polarized basis set are used for all atoms with a 75 Ry mesh cut-off [38]. The k-point samples are set to $1 \times 1 \times 40$ after the proper converge test. The most stable structures were found after optimizing till the force on each atom was lower than 0.01 eV/Å. The Grimme-DFT-D2 method used to consider van der Waals interaction effects.

It is still a challenge to propose a reliable model for understanding all the properties of graphene oxide nanoribbon. However, the model presented herein is maybe adequate for understanding the process of experiments done in this paper for gas sensing. A supercell containing six primitive unit cells of the zigzag GNR with the width of 7 is considered with hydrogen atoms at the edges. Then, a random generation code decided to change the bonds for each atom into different choices. These choices are to leave the bond intact, the vacancy defects (remove the atom), the oxygen bond, and –OH or –COOH groups. Then, optimized till the relaxed structure of GONR was achieved. Then, different sites are considered for the adsorption of NO_2 molecules.

To model MoS_2 nanospheres, a circle shape is selected from a multilayer supercell of MoS_2, transferred on the mentioned GONR to form a local heterostructure, and optimized.

4 Results and discussion

4.1 Characterization of GONRs

4.1.1 XRD of GONRs

The XRD of pristine multi-wall carbon nanotubes (MWCNTs) used for the synthesis of GONRs is shown in Fig. 2. In the XRD pattern of MWCNTs, a clear diffraction peak is observed at 26.1°, which relates to the characteristic (002) stacking peak corresponding to a d-spacing of 3.41 Å

between graphene sheets. The broad diffraction peak that appeared at 43.45 degrees is related to (100) stacking. After the longitudinal unzipping process, the (002) characteristic peak shifted to much lower 2θ values of 10.31° (related to a d-spacing of 8.65 Å) along with an evident broadening in the peak that shows the efficiency of the unzipping process and successful exfoliation of MWCNTs [39].

Another broad diffraction peak is in the XRD plot of unzipped carbon nanotubes (appeared at 43.45°) which shifted to 20° lower in the case of GONRs. This shift to lower intensity is related to the functional oxygen group bonded to the GONR sheet that led to an increase in the interlayer spacing of the graphitic structure [40, 41]. The Raman spectroscopy of MWCNTs and GONRs confirm these results, as shown in Supplementary S1.

4.1.2 TEM of GONRs

TEM images were obtained by drop-casting of a dilute solution of GONRs dispersed in DI water on the surface of a Cu grid with an electron beam of 300 kV**.** It is hard to distinguish between unzipped GONR and MWCNTs in the TEM image [38]. Hence, a figure to show the partial unzipping is considered to help such determine, as shown in Fig. 3. From the TEM images, the narrow graphene oxide nanoribbons formed via the longitudinal unzipping process are seen. The width of synthesized GONRs is 30–50 nm with a few micrometers in length.

4.2 Characterization of MoS_2 sphere

4.2.1 XRD analysis

Figure 4 shows the XRD of the as-synthesized MoS_2 nanoparticles black powder. The two weak, broadband diffraction peaks at 33.2° and 58.5° are related to the (100) and (110) peaks of pristine 2H-MoS_2 (JCPDS Card no. 73-1508). The diffraction peak in 14.5° is related to the periodic sequence of the MoS_2 layer in C axes which is a van der Waals bond. The shift in this peak may be related to the intercalation created during the fabrication process. This phenomenon can be helpful in further intercalation of gas molecules within MoS_2 edge bonds and improve its gas-sensing properties.

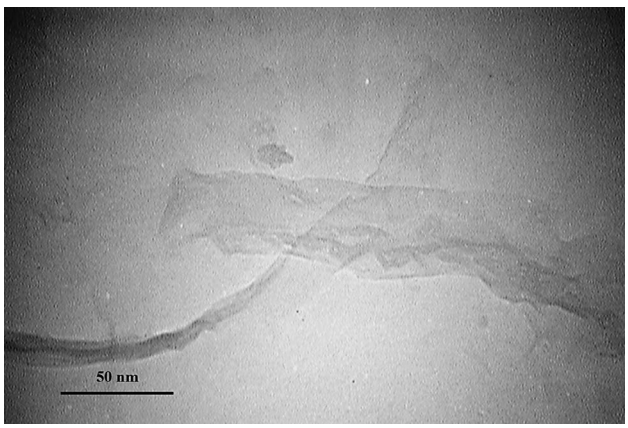

Fig. 3 The TEM image of unzipped carbon nanotube

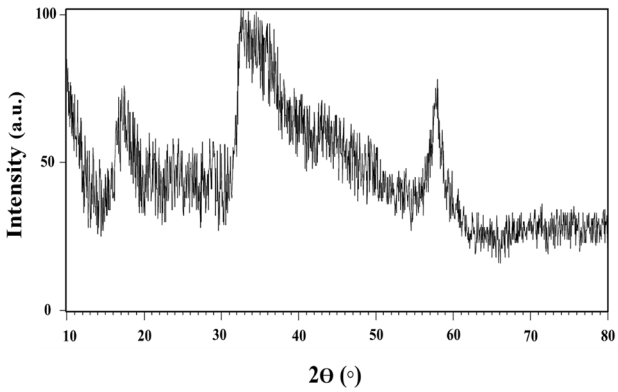

Fig. 4 The XRD of synthesized flower-shaped MoS_2 powder

4.2.2 SEM

The morphology of MoS_2 nanoparticles was investigated using scanning electron microscopy (SEM), and the image is depicted in Fig. 5. Considering the SEM image, the MoS_2 nanoparticles were formed from stacked MoS_2 nanosheets with a thickness of almost 20 nm. Moreover, this observation can further confirm the stacking effect observed in the XRD pattern of MoS_2 nanospheres.

4.3 Characteristic of final gas sensor

4.3.1 The FTIR

Figure 6 shows the FTIR of the pristine GONR compared with the MoS_2 nanospheres@GONRs. There are few resonance frequencies that excited and related to the MoS_2 and its bonds. However, no excited frequency due to the bond between MoS_2 and GONR can be seen, which shows that the van der Waals interaction are activated in the thin film.

4.4 Gas sensing of pristine GONR

The average resistance of the thin-film GONR used as the gas sensor is around 35kΩ with excellent stability in the air, as shown in Supplementary 2. The sensitivity vs. time of the pristine GONR thin-film sensor toward ten ppm of NO_2 gas is illustrated in Fig. 7a. The characteristic signals were systematically recorded in an air atmosphere at room

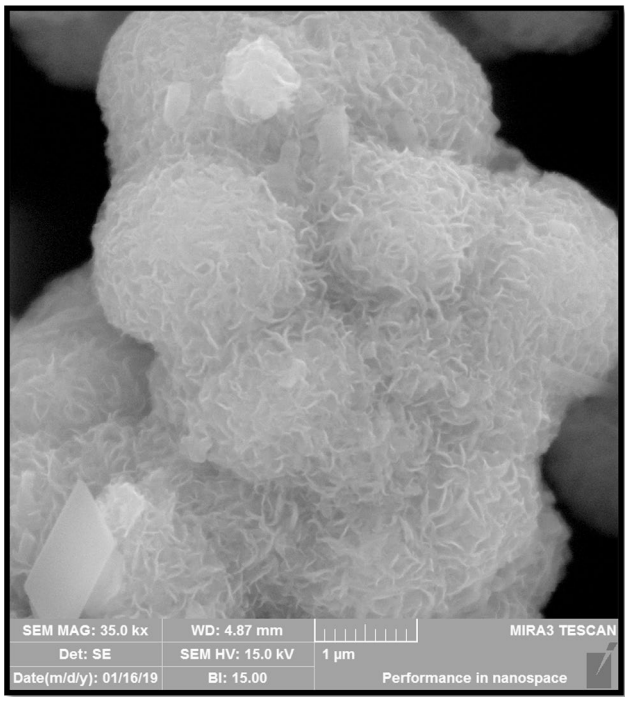

Fig. 5 SEM image of MoS_2 sphere-shaped nanoparticles

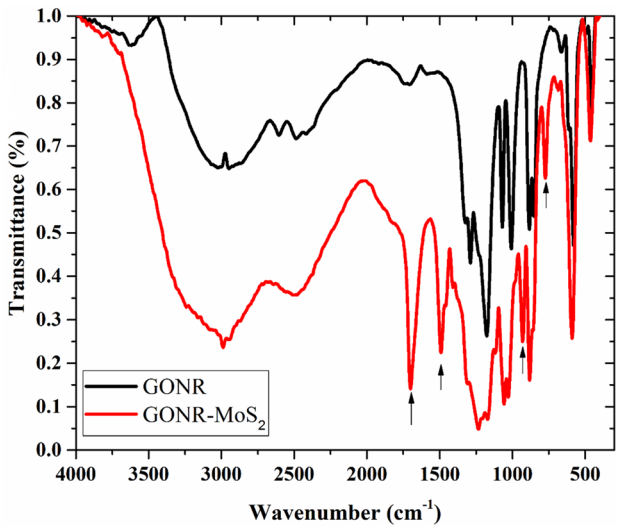

Fig. 6 the FTIR of the GONRs and MoS_2 nanospheres@GONRs

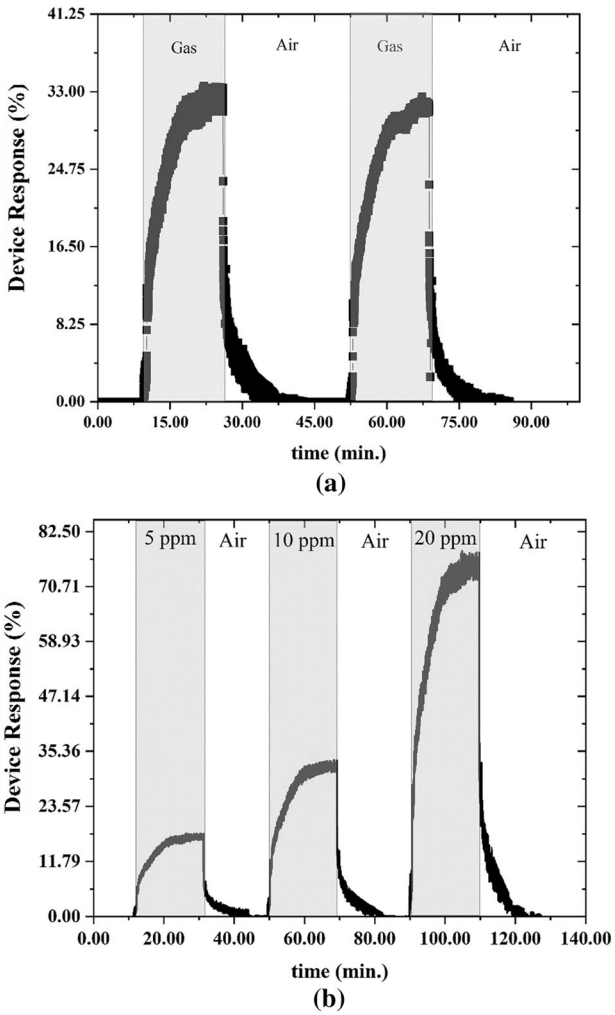

Fig. 7 The device response of thin-film GONR sensor vs. time toward **a** 10 ppm of NO_2, and **b** 5, 10, and 20 ppm of NO_2

Table 1 The sensitivity of the GONR thin-film gas sensor toward defined concentration (in ppm) of different dry gas molecules (25 °C, 5% humidity)

Gas	H_2S	CO_2	NH_3	H_2	CH_4
Sensor response %	10	7	9	5	5
ppm	10	10	20	100	100

temperature. When NO_2 was entered into the testing chamber, the sensor resistance decreased and a response value of approximately 33% was obtained for 10 ppm of NO_2. As the gas was exhausted from the chamber, the sensor almost returned to its initial values and was ready for the following gas-sensing sequence.

In addition, the response of the gas sensor toward lower and higher concentrations of NO_2 is also investigated and shown in Fig. 7b. The sensitivity toward 5 and 20 ppm of NO_2 is almost 18% and 76%, respectively. These results indicate a nearly linear response with a slope of 3.4, which was successfully used to predict the unknown concentration of gas in the chamber (Fig. 12c).

Table 1 shows the response of the pristine GONR gas sensor toward gas molecules other than NO_2. The sensitivity even for much higher concentration of different gas molecules is minimal.

4.5 Gas sensing mechanism of pristine GONR thin film

Regarding the response of the gas sensor toward NO_2, two distinct effects can be seen. First is the mechanism that led to the fast response of the gas sensor as the NO_2 molecules enter the chamber, and the second one is the slow exponential shape response. The first mechanism is slightly reduced in each run, while the second one did not show the same trend. To understand the mechanism, a very high concentration of gas was exposed to the gas sensor, and after 3 h, the response toward 10 ppm NO_2 was studied. In this case, only the second mechanism can be seen. Such an experiment shows that the first mechanism may be related to the structural defects of the system that naturalized with NO_2. Considering its moderately strong bond, it cannot be reactivated at room temperature.

Figure 8 illustrates the FTIR of thin-film GONR before and after exposure to NO_2 gas. The broad peak that appeared in 3190–3680 cm^{-1} is related to COOH and -OH groups, which shows the presence of oxygen functional groups on the basal and edge planes of GONR. After exposing the sample to NO_2 gas, two peaks with high intensity appeared in the range of 1000–1400 cm^{-1}. The peak at 1329 cm^{-1} and 1080 cm^{-1} is related to symmetric stretching of NO_2 at the defect sites and the C–N bond, respectively. Considering these differences after exposing the sample to NO_2 gas molecule, we can conclude that the nitrogen in NO_2 is occupied the defect sites on the GONR along with van der Waals interaction with the surface, which confirms two main mechanisms proposed for the detection of nitrogen oxide on the GONR thin layer.

In general, the Raman spectroscopy of graphene (oxide) nanoribbon is very similar to defected graphene (oxide) [42]. The GONR's Raman spectrum consists of two prominent peaks known as D and G. The G band is originated from sp^2 hybridization of carbon atoms inside the hexagonal structure of GONRs, and the D band is related to the sp and sp^3 hybridization and arose from the defects. The existence of the D band (Fig. 9) confirms the presence of defect sites in the basal plane of GONRs produced via the unzipping process of CNTs. In addition, it can reflect the reality of a high number of edge atoms [18]. The oxygen breaks the graphene hexagonal shape, and the G band is broadened, as seen in the GONR sample. By exposing the sample to NO_2, the G peak is shifted to lower values which can be resulted from two main reasons: first, the removal of the oxygen from the sample, which led to "self-repairing" of the carbon hexagonal structure, and second, due to the doping of the system with nitrogen [43]. It is reported that the intensity ratio of D:G peaks can be an effective tool to demonstrate the defect ratio in the carbon structures; such ratio is increased from 0.83 to 0.9 after exposure to the NO_2 molecules. This increment may be considered as the introduction of defects due to nitrogen atoms [43], or it may relate to the removal of oxygen from the thin layer that led to a decrease in the average size of the sp^2 domains with high intensity in the GONRs [44]. Some explanations of the affectivity of the D:G ratio and its relation to the defects can be found in the previous studies [42].

After exposing to NO_2 molecules, a change observed in the defects of the GONRs, which may relate to the replacing of C–C or C–O with C–N bonds that shifted the D peak [43]. Based on what had been discussed, it may be concluded

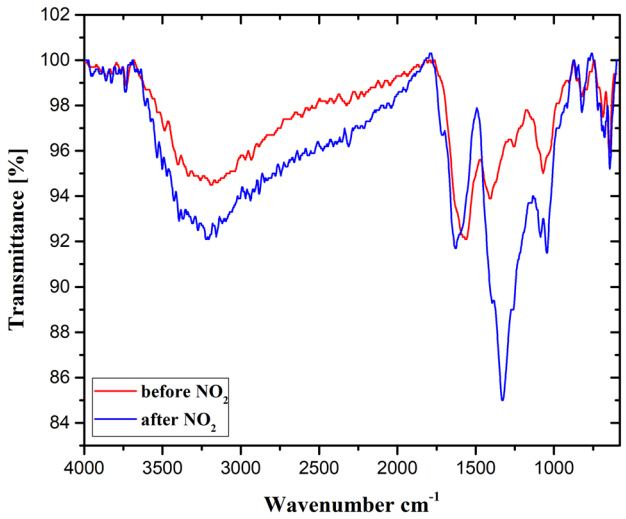

Fig. 8 The FTIR spectrum of thin-film GONR sensor before and after exposing to NO_2 in red and blue, respectively

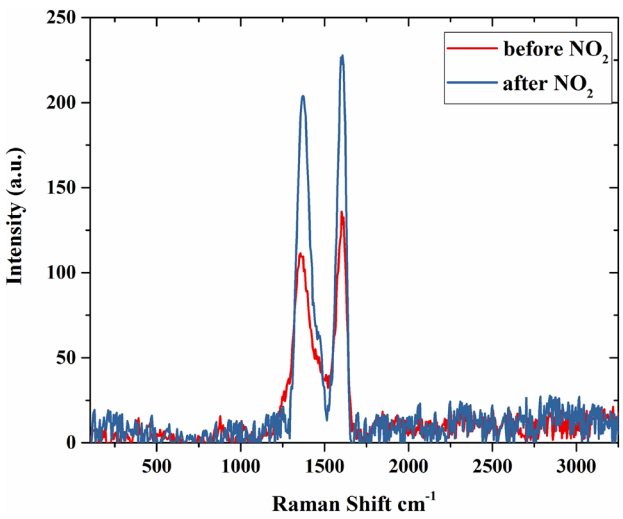

Fig. 9 The Raman spectroscopy of thin-film GONR sensor before and after exposing to NO_2 gas molecule in red and blue, respectively

that as the GONRs are exposed to the NO_2 molecules, and the nitrogen may remove the oxygen functional groups and simultaneously replace them at the defect centers of GONRs. Such results are in good agreement with our previous discussion on FTIR results.

4.6 Simulation

As mentioned earlier, proposing a proper model shows all the characteristics of GONR are still challenging. However, it seems that our homemade random model generator can correctly show the main properties of GONRs. To optimize the NO_2 molecular adsorption on GONR, different possible adsorption sites are considered. These adsorption sites were on the carbon, the oxygen, the –COOH, and the bridge between these sites. The most stable adsorption site is defined by considering the minimum total energy.

Figure 10a shows the optimized GONR with NO_2. As can be seen, the NO_2 molecule is bonded through one of its oxygen molecules to the carbon site. The bond length is 1.46 Å from the carbon to the oxygen, while the carbon to the nitrogen bond is 2.5 Å. As displayed in Fig. 10b, the electron density changes are illustrated from blue to red that indicates a gradual increase in electron density. A good electron polarization between NO_2 molecules and the GONR is observed which indicates partial charge transfer. Such transfer of charge may consider as the main reason for altering the current–voltage characteristic. Also, it represents the weak bond between NO_2 and GONR that can break easily, which agreed with reversible attitude of current–voltage characteristic in the presence and absence of the NO_2.

The optimized NO_2 molecule on defected GONR is illustrated in Fig. 10a. As can be seen, nitrogen atoms can form a strong covalence bond with carbons at the place

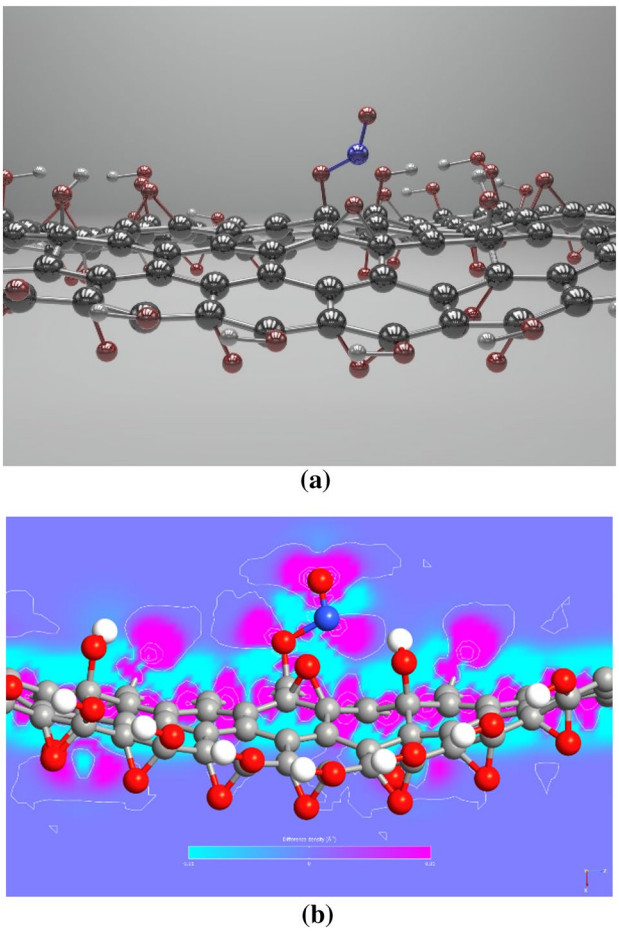

Fig. 10 **a** The relaxed structure and **b** electron density of GONR after NO_2 adsorption. The black, red, white, and blue balls are the carbon, the oxygen, the hydrogen, and the nitrogen atoms, respectively

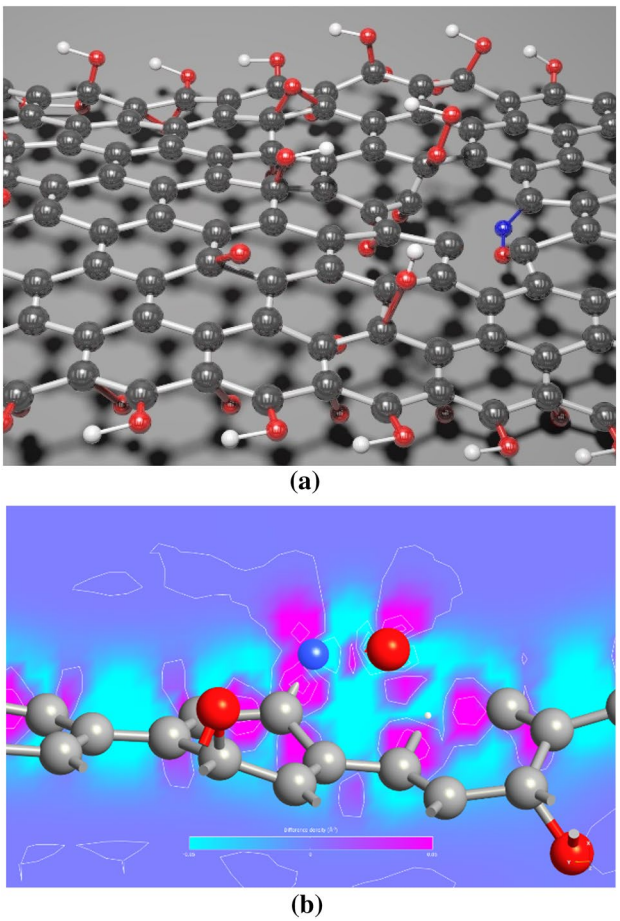

Fig. 11 **a** The relaxed structure and **b** electron density of defected GONR with NO_2 adsorption. The black, red, white, and blue balls are the carbon, the oxygen, the hydrogen, and the nitrogen atoms, respectively

of defects. Such a strong bond can alter the charge density as seen in differential electron density in Fig. 11b, which further confirms the transfer of charge at the defect sites. Such a charge transfer can modify the current–voltage characteristic, while the formed strong bond made it almost impossible to perform reversible responses at room temperature.

In short, the simulation results demonstrate the possibility of two mechanisms in detecting NO_2 as also achieved in the experiment. The defect sites act as a trap to perform irreversible charge transfer, while the pristine sites can adsorb the NO_2 in the chamber in a reversible manner.

4.7 Gas sensing of GONR decorated with MoS_2 nanospheres

The dynamic sensitivity versus time is illustrated in Fig. 12a for the thin film of GONR decorated with MoS_2 nanospheres. As 10 ppm of the NO_2 molecules were introduced into the testing chamber, the sensor resistance decreased immediately, and showed almost 250% sensitivity at room temperature. By exhausting the gas flow from the chamber, the sensor resistance changes to its initial condition and became ready for the next gas exposure step.

The response of the gas sensor toward lower and higher concentrations of NO_2 is also investigated and shown in

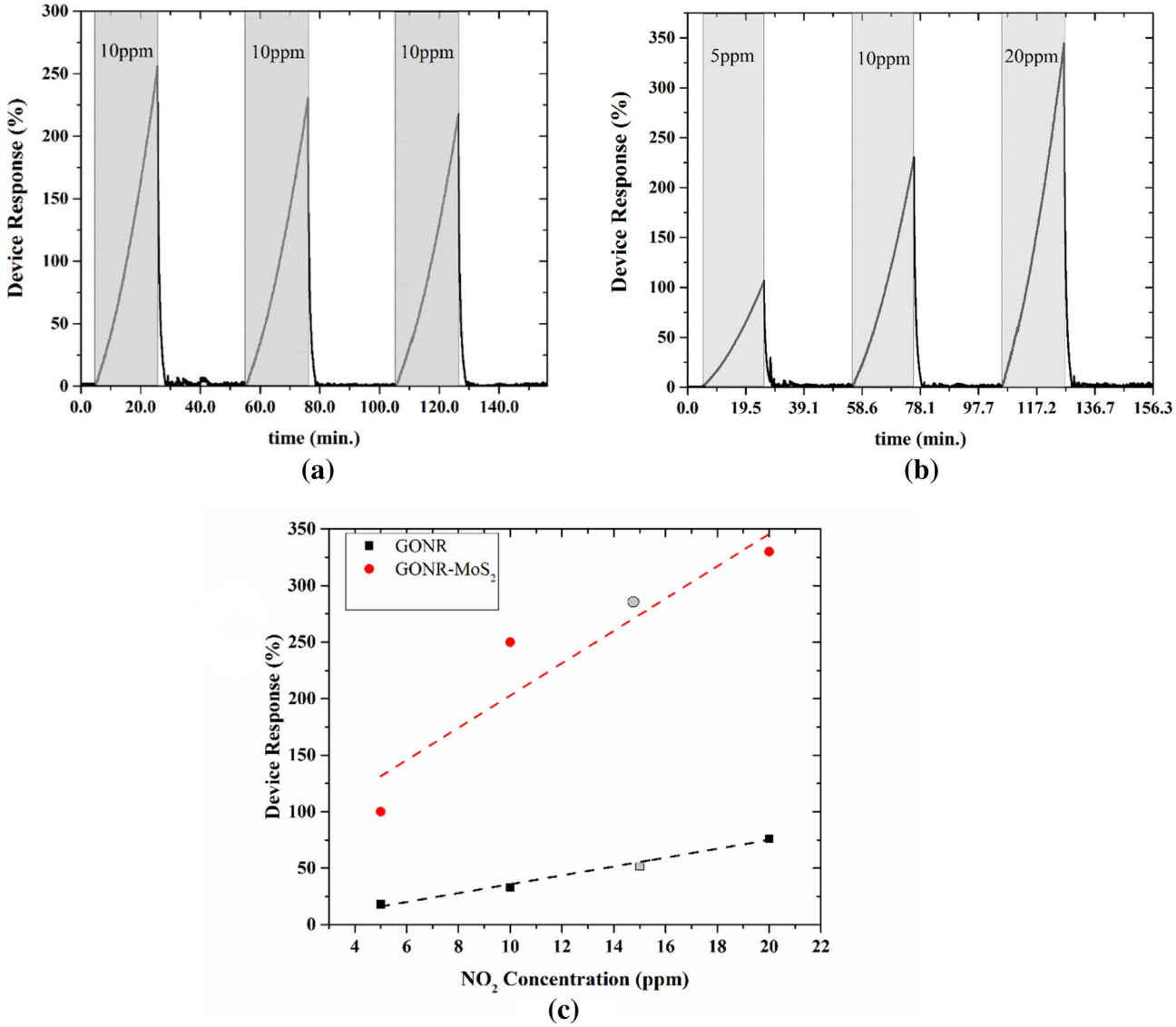

Fig. 12 The device response of thin-film GONR sensor decorated with MoS_2 nanospheres vs time toward **a** 10 ppm and **b** 5, 10, and 20 ppm of NO_2 at room temperature. **c** The device response vs. NO_2 concentration in ppm for GONR (black) and GONR–MoS_2 samples (red). The dark circle and square are first predicted, and then tested to show the accuracy of fitting lines

Fig. 12b. The characteristic responses obtained for 5 and 20 ppm of NO_2 were almost 100 and 330%, respectively. Modeling such response with a linear approximation of slope 20.1 and we can predict the unknown concentration of NO_2 in the chamber, as shown in Fig. 12c.

Compared with a similar situation for pristine GONR (Fig. 7), it is undeniable that MoS_2 nanospheres significantly improved the sensitivity toward the NO_2 gas molecules.

Table 2 shows the response of the MoS_2–GONR thin-film gas sensor toward other gas molecules, at room temperature. In comparison with pristine GONRs, the MoS_2 nanospheres improved the sensitivity toward all tested gases, while the selectivity toward the NO_2 is still appropriate.

4.8 Mechanism of gas sensing of MoS_2–GONR thin film

From Fig. 11, only one dominant process in the system is activated with NO_2. This process can be referred to the surface-to-volume ratio of the MOS_2 and the defects inside it. Such a high surface-to-volume ratio, can ease the charge transfer from NO_2 to MoS_2 [30]. The charge transfer from MoS_2 toward NO_2 has altered the Schottky barrier between MoS_2 and GONR and leads to remarkable sensitivity toward NO_2 gas molecules.

The defects, which are formed during the synthesis process, can be considered as active sites for detecting gas molecules. Few of these mentioned sites in MoS_2 and GONR are neutralized with the Nitrogen atoms, which slightly diminish the sensitivity of the gas sensor after repeating the gas-sensing cycles, as clearly seen in Fig. 11a.

Simulation can be considered helpful approach to enlighten our perspective on the adsorption process of NO_2 molecules on the surface of the modified electrodes. The circle-shaped MoS_2 is optimized and then transferred to the top of the GONR model. Next, the NO_2 was applied on the surface of MoS_2 at different places and fully optimized. The result is shown in Fig. 13a and the projected density of the state is shown in Fig. 13b, c, with and without NO_2, respectively.

The optimized structure is shown in Fig. 12a. As can be seen, charge transfer occurs at the positions where NO_2 molecules approach the MoS_2 surface. The bonds are formed at the defect sites, but the possible sites are the van der Waals charge transfer. These findings are in good agreement with the obtained experimental results.

In the case of the MoS_2–GONR system, the Schottky Barrier Height (SBH) is defined as the energy difference between the minimum conduction band (E_c) of MoS_2 and the Fermi level (E_f) [45]. Figure 13b, c displayed, the SBH of the sensor is almost 0.007 eV and 0.004 eV before and after NO_2 gas molecules, respectively. This change in the SBH shows that charge transfer from MoS_2 toward NO_2 is altering the barrier between GONR and MOS_2, and may lead to a change in the transport properties, which is in confirm with our experiments. In parallel with the experimental outcomes, for MoS_2 nanospheres@GONRs, only one primary mechanism was observed in simulation results.

In summary, the high surface-to-volume ratio provided by MoS_2 nanospheres on the surface of GONR improves the charge transfer between the sensor and the NO_2 molecules in the chamber, which alters the SBH between GONR and MoS_2 that consequently results in considerable sensitivity toward nitrogen dioxide gas molecules.

Table 3 compared the results of this paper with similar reports. As can be seen, the combination of GONR and MoS_2 improves the sensitivity of the flower-shape MoS_2 in gas sensing.

Table 2 The sensitivity of MoS_2–GONR thin-film gas sensor toward defined concentrations (in ppm) of different dry gas molecules (25 °C, 5% humidity)

Gas	H_2S	CO_2	NH_3	H_2
Sensor response %	121	76	77.5	55.3
ppm	10	10	20	100

5 Conclusions

The GONR thin-film and MoS_2 nanospheres@GONRs are introduced for detecting NO_2 gas molecules in low concentration, at room temperature. Narrow graphene oxide nanoribbons were utilized to modify combed shape gold electrodes on the silicon substrate. The MoS_2 nanospheres were synthesized through a hydrothermal route and used for GONR decoration by drop-casting on the GONR thin film. The pristine and decorated GONR thin film can detect 10 ppm of NO_2 with 33% and 250% sensitivity, at room temperature, respectively. By combining density functional theory along with XRD, TEM, SEM, FTIR, and Raman spectroscopy analysis, the mechanism of gas sensing was studied. It has been shown that detection in pristine GONR is almost due to the adsorption of gas molecules at the defect sites and charge transfer, while the change in the Schottky barrier is the dominant effect in the GONR–MoS_2 sensor. Our results show that the MoS_2 nanospheres@GONRs are good candidates for detecting the low concentration of nitrogen oxide at room temperature.

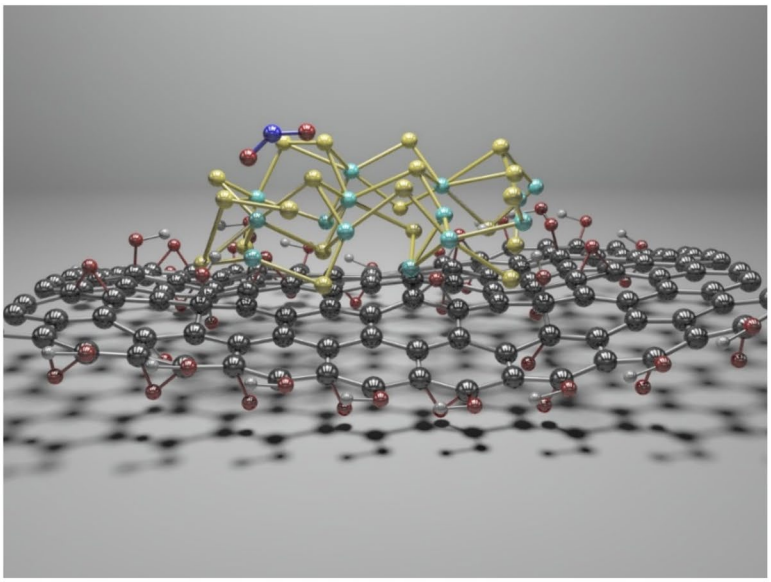

(a)

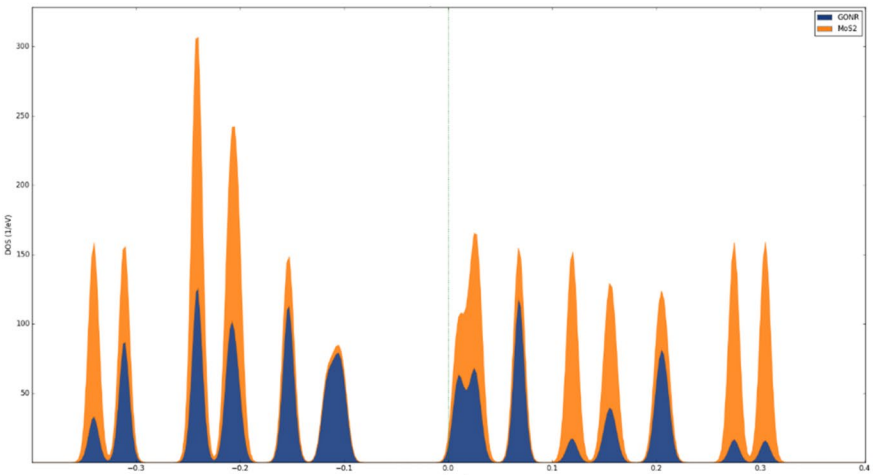

(b)

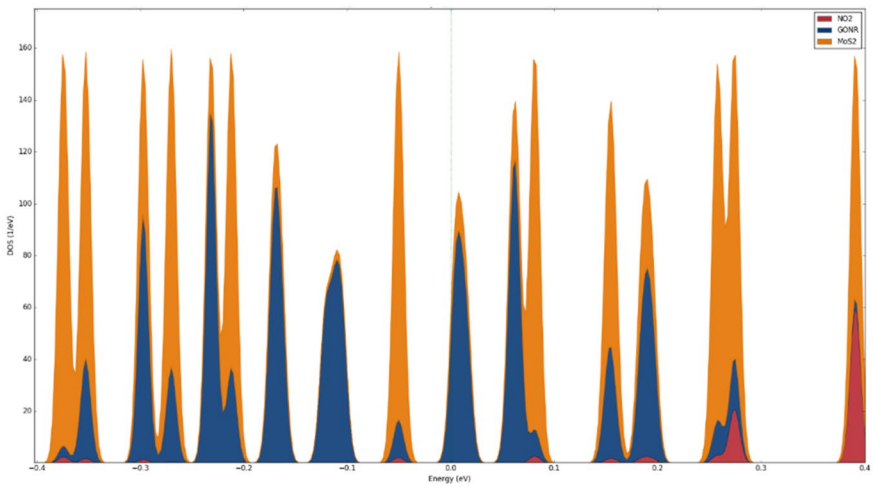

(c)

Fig. 13 **a** Optimized model for MoS_2–GONR in the presence of NO_2, **b** projected density of state for MoS_2–GONR, and **c** projected density of states for MoS_2–GONR in the presence of NO_2. The black, red, white, blue, yellow, and light-blue balls are the carbon, the oxygen, the hydrogen, the nitrogen, the sulfur, and the molybdenum atoms, respectively

Table 3 The sensitivity of this study compared with similar flower-shape

Sample	NO_2 concentration (ppm)	Sensitivity (%)	Temperature (in °C)
GONR	10	33	RT
GONR–MoS_2	10	250	RT
Flower shape MoS_2 [32]	10	10	100
Flower shape MoS_2 with In_2O_3[33]	10	20	RT
Metal-doped MoS_2 flowers [46]	Not main gas 10	7	RT
MoS_2–MoO_3–microflower [34]	10	33.6	RT
GONR–ZnO [27]	50	18	RT

Supplementary Information The online version contains supplementary material available at https://doi.org/10.1007/s00339-022-05605-x.

Acknowledgements We would like to thank E. Asadian Ph.D., for her consults, assistance in the growth of GONR, and for her comments that significantly improved the paper.

References

1. The National Institute for Occupational Safety and Health (NIOSH) CAS No. 10102-44-0
2. D.J. Jarvis, G. Adamkiewicz, M.E. Heroux, R. Rapp, F.J. Kelly, Nitrogen dioxide, WHO Guidelines for Indoor Air Quality: Selected Pollutants, p 201 (2010) ISBN: 9789289002134
3. L. Gao, Y. Jin, X. Liu, M. Xu, X. Lai, J. Shui, A rationally assembled graphene nanoribbon/graphene framework for high volumetric energy and power density Li-ion batteries. Nanoscale **10**, 7676–7684 (2018)
4. C. Xiang, W. Lu, Y. Zhu, Z. Sun, Z. Yan, C.C. Hwang, J.M. Tour, Carbon nanotube and graphene nanoribbon-coated conductive Kevlar fibers. ACS Appl. Mater. Interfaces **4**(1), 131–136 (2012)
5. A. Kauser, Poly(methyl methacrylate-co-methacrylic amide)-polyethyleneglycol/polycarbonate and graphene nanoribbon-based nanocomposite membranes for gas separation. Int. J. Polym. Anal. Charact. **23**(5), 450–462 (2018)
6. P. Jangid, D. Pathan, A. Kottantharayil, Graphene nanoribbon transistors with high I_{ON}/I_{OFF} ratio and mobility. Carbon **132**, 65–70 (2018)
7. S. Lone, A. Bhardwaj, A.K. Pandit, S. Gupta, S. Mahajan, A review of graphene nanoribbon field-effect transistor structures. J. Electron. Mater. **50**, 3169–3186 (2021)
8. L. Liang, V. Meunier, Atomically precise graphene nanoribbon heterojunctions for excitonic solar cells. J. Phys. Chem. C **119**(1), 775–783 (2015)
9. C. Xie, J. Jie, B. Nie, T. Yan, Q. Li, P. Lv, F. Li, M. Wang, C. Wu, L. Wang, L. Luo, Schottky solar cells based on graphene nanoribbon/multiple silicon nanowires junctions. Appl. Phys. Lett. **100**, 193103 (2012)
10. M. Berahman, M.H. Sheikhi, Optical excitations of finite length graphene nanoribbons. J. Comput. Theor. Nanosci. **8**(1), 90–96 (2011)
11. E. Salih, A.I. Ayesh, Enhancing the sensing performance of zigzag graphene nanoribbon to detect NO, NO_2, and NH_3 gases. Sensors **20**(14), 3932 (2020)
12. M. Shekhirev, A. Lipatov, A. Torres, N.S. Vorobeva, A. Harkleroad, A. Lashkov, V. Sysoev, A. Sinitskii, Highly selective gas sensors based on graphene nanoribbons grown by chemical vapor deposition. ACS Appl. Mater. Interfaces **12**(6), 7392–7402 (2020)
13. T.Y. Mi, D.M. Triet, N.T. Tien, Adsorption of gas molecules on penta-graphene nanoribbon and its implication for nanoscale gas sensor. Phys. Open **2**, 100014 (2020)
14. A. Mahmoudi, M. Troudi, Y. Bergaoui, P. Bondavalli, N. Sghaier, Analysis of simulated output characteristics of gas sensor based on graphene nanoribbon. J. Nanomater. **2016**, 9835340 (2016)
15. N. Harada, S. Sato, Electronic properties of NH_4-adsorbed graphene nanoribbon as a promising candidate for a gas sensor. AIP Adv. **6**, 055023 (2016)
16. D.V. Kosynkin, A.L. Higginbotham, A. Sinitskii, J.R. Lomeda, A. Dimiev, B.K. Price, J.M. Tour, Longitudinal unzipping of carbon nanotubes to form graphene nanoribbons. Nature **458**, 872–876 (2009)
17. A. Zehtab Yazdi, E.P.L. Roberts, U. Sundararaj, On the possibility of electrochemical unzipping of multiwalled carbon nanotubes to produce graphene nanoribbons. Mater. Res. Bull. **80**, 243–248 (2016)
18. A.L. Higginbotham, D.V. Kosynkin, A. Sinitskii, Z. Sun, J.M. Tour, Lower-defect graphene oxide nanoribbons from multiwalled carbon nanotubes. ACS Nano **4**, 2059–2069 (2014)
19. X. Shen, Y. Cui, Y. Pang, H. Qian, Graphene oxide nanoribbon and polyhedral oligomeric silsesquioxane assembled composite frameworks for pre-concentrating and electrochemical sensing of 1-hydroxypyrene. Electrochim. Acta **59**, 91–99 (2012)
20. G. Zhu, Y. Yi, B. Zou, Z. Liu, J. Sun, X. Wu, A glassy carbon electrode modified with a multiwalled carbon nanotube@reduced graphene oxide nanoribbon core-shell structure for electrochemical sensing of p-dihydroxybenzene. Microchim. Acta **182**, 871–877 (2015)
21. N.S. Ismail, Q. Hoa Le, H. Yoshikawa, M. Saito, E. Tamiya, Development of non-enzymatic electrochemical glucose sensor based on graphene oxide nanoribbon—gold nanoparticle hybrid. Electrochim. Acta **146**, 98–105 (2014)
22. J. Huan, Q. Liu, A. Fei, J. Qian, X. Dong, B. Qiu, H. Mao, K. Wang, Amplified solid-state electrochemiluminescence detection of cholesterol in near-infrared range based on CdTe quantum dots decorated multiwalled carbon nanotubes@reduced graphene oxide nanoribbons. Biosens. Bioelectron. **73**, 221–227 (2015)
23. A. Martín, P. Batalla, J. Hernández-Ferrer, M.T. Martínez, A. Escarp, Graphene oxide nanoribbon-based sensors for the simultaneous bioelectrochemical enantiomeric resolution and analysis of amino acid biomarkers. Biosens. Bioelectron. **68**, 163–167 (2015)
24. C. Sun, C. Su, J. Wu, Synthesis of short graphene oxide nanoribbons for improved biomarker detection of Parkinson's disease. Biosens. Bioelectron. **67**, 327–333 (2015)

25. Z. Wu, C. Li, J. Yu, X. Chen, MnO_2/reduced graphene oxide nanoribbons: facile hydrothermal preparation and their application in amperometric detection of hydrogen peroxide. Sens. Actuators B Chem. **239**, 544–552 (2017)
26. H. Abdollahi, M. Samkan, M. Bayat, Graphene oxide nanoribbons for ethanol detection at room temperature. Mater. Res. Express **6**, 075053 (2019)
27. C. Wang, L. Zhang, H. Huang, R. Xi, D. Jiang, S. Zhang, L. Wang, Z. Chen, G. Pan, A nanocomposite consisting of ZnO decorated graphene oxide nanoribbons for resistive sensing of NO_2 gas at room temperature. Microchim. Acta **186**, 554 (2019)
28. H. Ahmadvand, A. Irajizad, R. Mohammadpour, S.H. Hosseini-Shokouh, E. Asadian, Room temperature and high response ethanol sensor based on two-dimensional hybrid nanostructures of WS2 GONRs. Sci. Rep. **10**. Article number 14799 (2020)
29. H. Xu, Y. Li, N. Huang, Z. Yu, P. Wang, Z. Zhang, Q. Xia, L. Gong, S. Li, L. Zhao, G. Zhang, L. Tang, Temperature-triggered sensitive resistance transition of graphene oxide wide-ribbons wrapped sponge for fire ultrafast detecting and early warning. J. Hazard. Mater. **363**(5), 286–294 (2019)
30. B. Cho, M.G. Hahm, M. Choi, J. Yoon, A.R. Kim, Y.J. Lee, S.G. Park, J.D. Kwon, C.S. Kim, M. Song, Y. Jeong, K.S. Nam, S. Lee, T.J. Yoo, C.G. Kang, B.H. Lee, H.C. Ko, P.M. Ajayan, D.H. Kim, Charge-transfer-based gas sensing using atomic-layer MoS_2. Sci. Rep. **2015**, 8052 (2015)
31. M. Barzegar, M. Berahman, A. Iraji zad, Sensing behavior of flower-shaped MoS_2 nanoflakes: case study with methanol and xylene. Beilstein J. Nanotechnol. **9**, 608–615 (2018)
32. Y. Zhang, W. Zeng, Y. Li, Hydrothermal synthesis and controlled growth of hierarchical 3D flower-like MoS_2 nanospheres assisted with CTAB and their NO_2 gas sensing properties. Appl. Surf. Sci. **455**, 276–282 (2018)
33. D. Zhang, C. Jiang, J. Wu, Layer-by-layer assembled In_2O_3 nanocubes/flower-like MoS_2 nanofilm for room temperature formaldehyde sensing. Sens. Actuators B Chem. **273**, 176–184 (2018)
34. R. Kumar, N. Goel, M. Mishra, G. Gupta, M. Fanetti, M. Valant, M. Kumar, Growth of MoS_2–MoO_3 hybrid microflowers via controlled vapor transport process for efficient gas sensing at room temperature. Adv. Mater. Interfaces **5**(10), 1800071 (2018)
35. C.P. Veeramalai, F. Li, H. Xu, T.W. Kim, T. Guo, One-pot hydrothermal synthesis of graphene-like MoS_2 nanosheets for application in high performance lithium ion batteries. RSC Adv. **5**, 57666–57670 (2015)
36. A. García, N. Papior, A. Akhtar, E. Artacho, V. Blum, E. Bosoni, P. Brandimarte, M. Brandbyge, J.I. Cerdá, F. Corsetti, R. Cuadrado, V. Dikan, J. Ferrer, J. Gale, P. García-Fernández, V.M. García-Suárez, S. García, G. Huhs, S. Illera, R. Korytár, P. Koval, I. Lebedeva, L. Lin, P. López-Tarifa, S.G. Mayo, S. Mohr, P. Ordejón, A. Postnikov, Y. Pouillon, M. Pruneda, R. Robles, D. Sánchez-Portal, J.M. Soler, R. Ullah, V. Wen-zhe Yu, J. Junquera, Siesta: recent developments and applications. J. Chem. Phys. **152**, 204108 (2020)
37. K. Stokbro, J. Taylor, M. Brandbyge, P. Ordejon, TranSIESTA: a spice for molecular electronics. Molecular electronics III. Ann. New York Academy Sci. **1006**(1), 212–226 (2013)
38. P. John, Perdew, Kieron Burke, and Matthias Ernzerhof, generalized gradient approximation made simple. Phys. Rev. Lett. **78**, 1396 (1999)
39. C. Chang, K. Chang, H. Shen, C. Chang, A unique two-step Hummers method for fabricating low-defect graphene oxide nanoribbons through exfoliating multiwalled carbon nanotubes. J. Taiwan Inst. Chem. Eng. **45**(5), 2762–2769 (2014)
40. J. Al Dream, C. Zequine, K. Siam, P.K. Kahol, S.R. Mishra, R.K. Gupta, Electrochemical properties of graphene oxide nanoribbons/polypyrrole nanocomposites. C J. Carbon Res. **5**(2), 18 (2019)
41. E. Castillo-Martínez, J. Carretero-González, J. Sovich, M.D. Lima, High temperature structural transformations of few layer graphene nanoribbons obtained by unzipping carbon nanotubes. J. Mater. Chem. A **2**, 221–228 (2014)
42. C. Casiraghi, D. Prezzi, Raman spectroscopy of graphene nanoribbons: a review. GraphITA, pp. 19–30 (2017) (ISBN: 9783319581347)
43. Z. Sheng, L. Shao, J. Chen, W. Bao, F. Wang, X. Xia, Catalyst-free synthesis of nitrogen-doped graphene via thermal annealing graphite oxide with melamine and its excellent electrocatalysis. ACS Nano **5**(6), 4350–4358 (2011)
44. S. Stankovich, D.A. Dikin, R.D. Piner, K.A. Kohlhaas, A. Kleinhammes, Y. Jia, Y. Wu, S.T. Nguyen, R.S. Ruoff, Synthesis of graphene-based nanosheets via chemical reduction of exfoliated graphite oxide. Carbon **45**(7), 1558–1565 (2007)
45. S.S. Baik, S. Im, H.J. Choi, Work function tuning in two dimensional MoS_2 field-effect transistors with graphene and titanium source-drain contacts. Sci. Rep. **7**, 45546 (2017)
46. D. Zhang, J. Wu, P. Li, Y. Cao, Room-temperature SO_2 gas-sensing properties based on a metal-doped MoS_2 nanoflower: an experimental and density functional theory investigation. J. Mater. Chem. A **5**, 20666–20677 (2017)